

# Pressure-stabilized Planar N<sub>4</sub>-ring and Bonding Properties in Manganese Nitrides

Li Li<sup>1</sup>, Kuo Bao<sup>1\*</sup>, Xingbin Zhao<sup>1</sup>, and Tian Cui<sup>2,1\*</sup>

<sup>1</sup>State Key Laboratory of Superhard Materials, College of Physics, Jilin University, Changchun, 130012, China

<sup>2</sup>School of Physical Science and Technology, Ningbo University, Ningbo, 315211, China

\*Corresponding authors: [baokuo@jlu.edu.cn](mailto:baokuo@jlu.edu.cn), and [cuitian@jlu.edu.cn](mailto:cuitian@jlu.edu.cn)

## Abstract

Manganese nitrides should be with amazing properties and promised application, because manganese atom is particular for its magnetism, valence states, high electron density, etc., and N atoms in compounds form different substructures. It is hard to good synthesize manganese nitride crystals with all established means, therefore, theoretical studies are highly welcome. In this study, we systematically examined the stoichiometric phases spaces of Mn-N compounds from 0 to 100 GPa based on *ab initio* calculations, and constructed the high-pressure magnetic phase diagram. Remarkably, N-rich MnN<sub>4</sub> with a planar N<sub>4</sub> ring was discovered for the first time in the pressure range from 40 to 100 GPa. The electronic structures reveal that the N<sub>4</sub> ring is driven by the *sp*<sup>2</sup> hybridization of nitrogen atoms. This phase with  $T_c \approx 1.6$  K and high bulk modulus  $B = 381$  GPa, which make it potentially interesting as a hard superconductive material. Moreover, the phase transition sequence for the MnN compound is summarized renewedly, the semi-conducting NM-*zb* phase (5 GPa) first transforms to metallic AFM-*NiAs* (40 GPa), which further transforms to the more stable metallic FM-*rs* phase. The mechanical properties show that covalent interaction has a great effect on N-rich structures' hardness and hardly effect on Mn-rich structures in Mn-N compounds.

**Keywords:** Transition metal nitrides; Superconductivity; Mechanical properties; Electronic properties; Magnetic

## Introduction

Synthesis of “pure” transition metal (TM) nitrides or compounds with an integral ratio is a challenge by conventional high temperature methods, because nitrogen ( $N \equiv N$ ) is highly stable and unreactive at ambient pressure and room temperature. Consequently, exploration and application of this kind of nitride materials are seriously hindered and limited. High pressure (HP) is an effective and clean method to change hybridization modes, bonding ways, and valence electron orbits and synthesize novel material with special physicochemical properties, especially in TM nitrides. A series of poly-nitrogen forms have been predicted and synthesized at HP. Such as, the armchairlike hexazine ( $N_6$ ) rings,<sup>1</sup> the pentazolate cyclo- $N_5^-$ ,<sup>2</sup> the  $N_2$  and  $N_6$  unit,<sup>3</sup> and other N-chains.<sup>3-5</sup> In addition to high energy density materials, TM nitrides have been drawing considerable attention owing to the outstanding mechanical<sup>6</sup>, superconductive, and magnetic properties in them under certain conditions. TiN was synthesized as a superconducting film that underwent disorder-driven superconductor–insulator transition.<sup>7</sup> The NbN<sup>8-9</sup> and MoN<sup>10</sup>, even, as ultra-hard and superconducting unconventional functional nitrides have been reported. A large number of works have shown that different ways of bonding between nitrogen atoms have important effects on the mechanical properties of materials. In the Fe–N system, the hardness of  $Fe_3N_8$  and  $FeN_3$  with N chains was above 30 GPa.<sup>3</sup> Recently, trigonal  $WN_6$  with armchair-like hexazine ( $N_6$ ) rings was synthesized, and the hardness was determined to be 57.9 GPa by theoretical calculations.<sup>1</sup> The  $N_2$  units in  $CrN_2$ ,  $TiN_2$ ,  $IrN_2$  and  $OsN_2$  impart ultra-incompressible with high bulk modulus (B) and shear modulus (G).<sup>6, 11</sup>

Mn is magnetic element, Mn–N compounds have rich magnetic phases. Until now, the  $\epsilon$ - $Mn_4N$ ,  $\zeta$ - $Mn_2N$ ,  $\theta$ - $MnN$ , and  $\eta$ - $Mn_3N_2$  have been synthesized<sup>12-14</sup>. Face-centered cubic  $\epsilon$ - $Mn_4N$  performs interesting FiM order magnetism, which the magnetic moment of Mn on the corner (Mn-I) is  $3.3 \mu_B$  and antiparallel to the three Mn (Mn-II) on face center  $0.7 \mu_B$ <sup>15</sup>. It exhibit distinct anomalous Hall Effect in perpendicular magnetic fields<sup>16-17</sup> and show extremely high Curie temperature about 710 K<sup>18</sup>. The  $\zeta$ - $Mn_2N$  formed a  $\zeta$ - $Fe_2N$  type AFM orthorhombic phase and neutron diffraction experiment confirm the space group (SG) is  $Pbcn$  with the lattice constant  $a = 5.668 \text{ \AA}$ ,  $b = 4.909 \text{ \AA}$ ,  $c = 4.537 \text{ \AA}$ <sup>19</sup>. Later, experimentally by using an In-Na flux at 700 °C and 5 MPa of  $N_2$  prepare the  $P6_3/mmc$ - $Mn_2N_{1.06}$ <sup>13</sup>.  $\eta$ - $Mn_3N_2$ , a tetragonal ( $I4/mmm$ ) metal with the lattice constant  $a = 2.994$ ,  $c = 12.499 \text{ \AA}$ <sup>20</sup> and Néel temperature of 925K<sup>21</sup>. The magnetic moment is parallel aligned in (001) plane, lie along the [100] direction and performed AFM order along [001]. Due to the high reversible capacity and good cycle performance, it could be an anode material for lithium-ion batteries<sup>22</sup>. However, the ground state structure of MnN has always been discussed.  $\theta$ -MnN exists experimentally in a tetragonally distorted rock salt (*rs*) structure with AFM order. It perform metal property with lattice parameters  $c/a = 0.984$  in the [001] direction and magnetic moment of Mn atom is  $3.3\mu_B$  at 0 K<sup>23</sup>. However, a mass of theories have been reported for the hypothetical cubic zinc-blende (*zb*). A. Janotti *et al*<sup>24</sup> explained why the ground state *zb*-AFM state has larger lattice constant and higher magnetic moment of Mn atom than ferromagnetic (FM) phase. Hong *et al* studied Mn and VA (N, P, As, Sb) binary compounds in the *NiAs* and *zb* phases and reported that the ground state is AFM *zb* phase, because the energy of N-*p* level is much lower than other anions *p* and more likely to form a lower coordination number *zb* phase. Meanwhile, the AFM ordering have lager volume so that reduced the *p-d* and *d-d* coupling, so the AFM state is more stable<sup>25</sup>. However, compared with iron nitrides that forming abundant N-rich Fe–N compounds under HP, like  $FeN_2$ ,  $FeN_4$ ,  $Fe_3N_8$ , the N-rich Mn–N are also worth investigating.

In this study, we investigated Mn–N compounds from 0 to 100 GPa based on *ab initio* calculations. A series of new N-rich magnetic phases are predicted. Remarkably, a new bonding pattern for N (planar  $N_4$  rings) is discovered for the first time in  $MnN_4$  and the bonding properties have been analyzed, and it could be a potentially

hard superconductive material. Moreover, the phase transition sequence for MnN is determined renewedly. Finally, the incompressibility of all the structures of the Mn–N compounds was determined.

## COMPUTATIONAL METHODS AND DETAILS

The structural searching for Mn–N compounds are based on the evolutionary algorithm with spin-polarized using the variable-composition mode of the USPEX code<sup>26-27</sup> at 0, 50, 100 GPa. Structural relaxations, electronic properties, and total energies were calculated on density functional theory (DFT) as implemented in the Vienna ab initio simulation package<sup>28</sup> with the project augmented waves method.<sup>29</sup> And the Perdew-Burke-Ernzerhof parametrization of the generalized gradient approximation was used.<sup>30</sup> A cutoff energy of 850 eV was chosen. Monkhorst-Pack k-grid meshes<sup>31</sup> with a reciprocal space resolution of  $2\pi \times 0.03 \text{ \AA}^{-1}$  and  $2\pi \times 0.02 \text{ \AA}^{-1}$  were used for thermodynamic calculations and electronic property determination, respectively. The electronic configurations of  $3d^64s^1$  and  $2s^22p^3$  are chosen in Mn and N, respectively. Phonon dispersion curves with PHONOPY code<sup>32</sup> based on a supercell approach with the force-constant matrices and electron-phonon coupling were performed by density functional perturbation theory as implemented in the Quantum ESPRESSO package.<sup>33</sup> Norm-conserving potentials were used with a kinetic energy cutoff of 90 Ry. And the q-point mesh of the electron-phonon interaction matrix element adopted  $4 \times 4 \times 4$  in  $\text{MnN}_4$ . Elastic constants are calculated using the strain stress method, while bulk modulus (B) and shear modulus (G) and are derived from the Voigt–Reuss–Hill averaging scheme.<sup>34</sup>

## Results and discussion

### 3.1. Phase Stability of Mn–N Compounds at High Pressure.

Formation enthalpies ( $\Delta H_f$ ) from the global energy minimum of the Mn–N system were computed from the convex hull.  $\Delta H_f$  of each structure was calculated using the following relation:  $\Delta H_f(\text{Mn}_x\text{N}_y) = [H(\text{Mn}_x\text{N}_y) - xH(\text{Mn}) - yH(\text{N})]/(x+y)$  ( $x, y = 0, 1, 2, \dots$ ). The  $\alpha$ -Mn and low-energy N phases ( $\alpha$ , *Pbcn*, *P2/c*, and *cg* phases) at different pressures were used as the reference phases.<sup>35</sup> To the best of our knowledge, pressure – composition magnetic phase diagrams of the Mn–N system have not been reported yet. In the pressure range 0-100 GPa,  $\text{Mn}_3\text{N}$ ,  $\text{Mn}_2\text{N}$ ,  $\text{Mn}_3\text{N}_2$ , MnN,  $\text{MnN}_2$ , and  $\text{MnN}_4$  are the stable phases. The experimentally determined cubic  $\text{Mn}_4\text{N}$  phase<sup>16, 36</sup> is located above the convex hull at all the time (**Figure 1a,b**). The lattice constants are listed in **Table S1**. In terms of structures of Mn–N compounds, with increasing nitrogen content, the layer structures in MnN compounds transform into polyhedral structures centered around the Mn atom (**Figure S1**). The metastable phases (dynamically and mechanically stable phases, namely, NM-*C2/m*- $\text{Mn}_3\text{N}$  and NM-*Cmmm*- $\text{MnN}_4$ ) by structure search are worth studying because they could be synthesized experimentally, like the AFM *Pbcn*- $\text{Mn}_2\text{N}$ .<sup>19, 37</sup> The corresponding structure diagrams are shown in **Figure S2**, and the phonon spectra are shown in **Figure S3** and **S4**. Three stable Mn-rich manganese polynitrides are predicted. For  $\text{Mn}_2\text{N}$ , experimental studies proposed an *Pbcn* phase. Examination of the relative enthalpy (**Figure S5**) reveal that *P6<sub>3</sub>/mmc*- $\text{Mn}_2\text{N}$ , obtained through our structure search, has lower energy. *R $\bar{3}m$* - $\text{Mn}_3\text{N}_2$  is first predicted to be thermodynamically stable from 17 to 100 GPa, since *R $\bar{3}m$* - $\text{Mn}_3\text{N}_2$  is dynamically unstable below 10 GPa; the ground state is the experimentally determined AFM-*I4/mmm* phase at 0 GPa. *P $\bar{6}m2$* - $\text{Mn}_3\text{N}$  and *P6<sub>3</sub>/mmc*- $\text{Mn}_2\text{N}$  are stable from 0 to 100 GPa. For  $\text{MnN}_4$ , the NM-*Immm* can be obtained by the decomposition of  $\text{MnN}_2$  (**Figure 1b**), and it can remain stable at 40-100 GPa. From the phase diagram (**Figure 1c**), the NM-*zb* phase first transforms to AFM-*NiAs* at 5 GPa, which further transforms to the more stable FM-*rs* phase at 40 GPa. For the  $\text{MnN}_2$ , it will be

reported in another work.

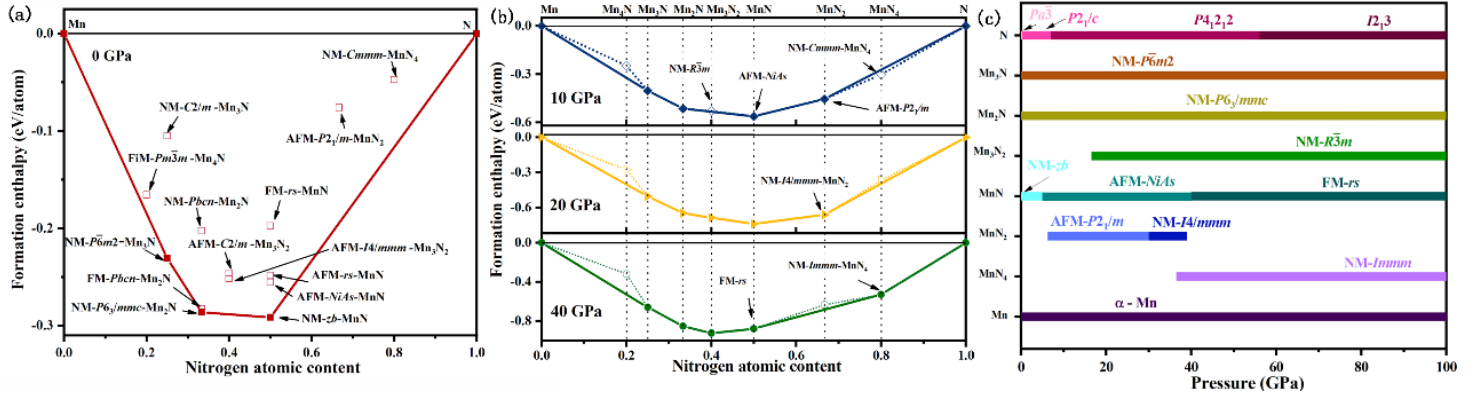


**Figure 1.** The magnetic phases (i.e., NM, FM, and AFM) of thermodynamic stability and the stable pressure ranges of Manganese nitrogen system. (a),(b) Convex hull diagram of the Mn–N system at different pressures at 0K. The solid squares connected by solid lines on the convex hull are represent thermodynamics and dynamics stable. (c) Pressure-composition phase diagram of the Mn–N system.

### 3.2. Bonding, Electronic, and Superconductive Properties of NM-*Immm*-MnN<sub>4</sub> Phase with N<sub>4</sub> Rings

Although NM-*Immm*-MnN<sub>4</sub> phase can't remain to ambient pressure, the novel bonding way of N atoms is worth studying. The structure contains MnN<sub>6</sub> octahedrons that are connected by N atoms (**Figure 2a**). Previously, cyclo-N<sub>5</sub><sup>-</sup>, N<sub>3</sub> units, and N<sub>6</sub>-rings and N<sub>x</sub> (x = 3, 4 ...) chains have been identified in nitrides,<sup>2-3, 5, 37</sup> however, it is unusual that the N atoms form 4-membered rings in this structure. To the best of our knowledge, there are no studies demonstrating the existence of planar N<sub>4</sub> rings in TM nitrides. In **Figure 2b**, the ELF of this phase is calculated for bonding analysis and it is valid for determining bonding characters, such as, covalent, metallic, ionic bonds and lone pairs. The results of ELF show the strong electronic localization between adjacent N1-N2 within the planar N<sub>4</sub> rings with the scale larger than 0.75. This is implying covalent bonds in N1-N2 and the N atoms are in the *sp*<sup>2</sup> hybridization. The N1-N2 bond length in the N<sub>4</sub> rings is 1.380 Å, which is extremely close to the N-N single bond at 40 GPa. The Mn-N1 and Mn-N2 bond length are 1.930 and 1.807 Å, respectively.

Moreover, the crystal orbital Hamilton population COHP (ICOHP) have been analyzed to characterize the bonding in MnN<sub>4</sub> are showed in **Figure 2c**. The COHP plot of the N1–N2 pairs suggest that bonding states are fully occupied between energy range (-12 - -4 eV) and partially occupy on antibonding states, it is leading to covalent bonding between N1–N2 of N<sub>4</sub> rings. There is also some covalent interaction between Mn and N due to the partially occupy on bonding states. The value of ICOHP reflect the bond strength, the interaction between N1–N2 is strongest (-ICOHP = 12.024); the Mn-N1 (-ICOHP = 4.101) and Mn-N2 (-ICOHP = 2.848) are second; the Mn-Mn (-ICOHP = 0.681) is weakest. Furthermore, the Laplacian of the charge density at the critical point was calculated to analyze the bonding behavior derived from a QTAIM<sup>38</sup>. The BCP between N1 and the nearest N2 possesses an electron density ( $\rho(r)$ ) of 2.418 a.u. and a Laplacian ( $\nabla^2\rho(r)$ ) of -20.255 a.u., indicating stronger covalent interactions due to positive  $\rho(r)$  and negative  $\nabla^2\rho(r)$ . This result is quite in line with COHP and ELF. The BCP between Mn and the nearest N1 (N2) possesses a  $\rho(r)$  of 0.678 a.u. (0.678 a.u.) and a  $\nabla^2\rho(r)$  of 14.321 a.u. (11.323 a.u.). The positive  $\rho(r)$  and  $\nabla^2\rho(r)$  imply that there is not entirely closed-shell interaction between Mn and N atoms, and there are partial charge transfer bonds.<sup>39</sup> Actually, the Bader charge analysis reveals that per Mn atom loses  $\sim 1.2 e^-$  to adjacent N atoms.

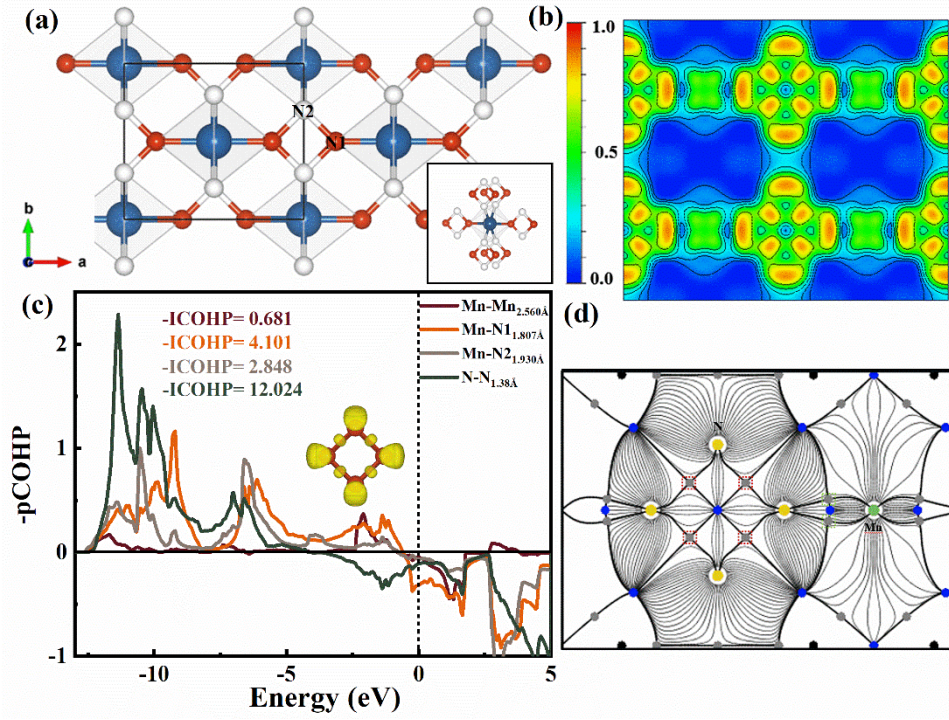


**Figure 2.** Crystal structures and electronic properties of MnN<sub>4</sub>. (a) Crystal structure. Blue, red and white spheres denote Mn, N1 and N2 atoms. (b) The electron local function (ELF). (c) The COHP, positive values represent bonding states, zero means nonbonding state, and negative values represent anti-bonding state. Inset represents the planer N<sub>4</sub> ring with an isosurface value of 0.8. (d). Gradient paths and critical points derived from QTAIM analysis for MnN<sub>4</sub>, gray spheres represent BCPs, yellow spheres represent N, and green spheres represent Mn. Gray spheres in red dashed line boxes represent BCPs between N and N, in green dashed line boxes represent BCPs between Mn and N.

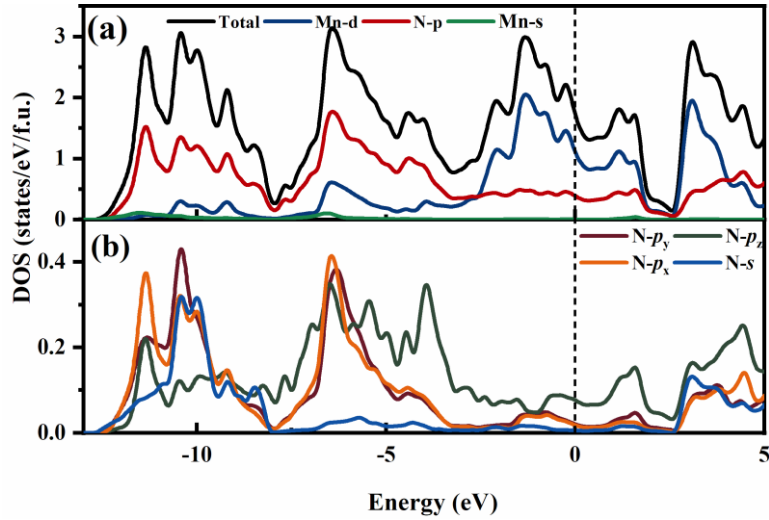


**Figure 3.** Projected DOS of NM-*Immm* at 40 GPa.

To understand the formation mechanism of the novel NM-*Immm*-MnN<sub>4</sub>, the calculated DOS are shown in **Figure 3**, the Mn-3*d* orbital plays a dominant role on the Fermi level and between the energy range from -13 to -2.5 eV, dominated by N-*p*. The *s*, *p<sub>x</sub>*, and *p<sub>y</sub>* orbitals of N-*p* have the same peak energy, indicating that these orbitals of each N atoms form three *sp*<sup>2</sup> hybridized orbitals for the N<sub>4</sub> rings, while the two *sp*<sup>2</sup> orbitals of each N atom form two  $\sigma$  bonds with the *sp*<sup>2</sup> hybridized orbitals of two neighboring N atoms. The extra *sp*<sup>2</sup> orbitals form lone pairs (see the ELF in inset of **Figure 2c**), while the four *p<sub>z</sub>* orbitals form delocalized  $\pi$  bonds (**Figure 3b**).



The Mn-4s profile throughout this range of energy is very small, indicating charge transfer from Mn to N. Thus, the partially electrons filled the  $\pi$ -antibonding states impart metallicity and promote the mutual interaction between Mn and N, which too results in a metallic state. This also confirmed the results of COHP.

Due to the sizable DOS at the Fermi level of NM-*Immm*-MnN<sub>4</sub>, we estimated the superconducting transition temperature ( $T_c$ ) at 40 GPa. The phonon spectrum, PHDOS, and Eliashberg spectral function  $\alpha^2F(\omega)$  together with the electron-phonon integral  $\lambda$  of NM-*Immm* at 40 GPa are showed in **Figure 4**. The EPC parameters, namely,  $\lambda \approx 0.41$  and  $T_c \approx 1.6$  K using the McMillan equation modified by Allen and Dynes. NM-*Immm*-MnN<sub>4</sub> is weak-coupling superconductivity. Combine with the COHP and DOS, the interaction between Mn and N is the main contribution.

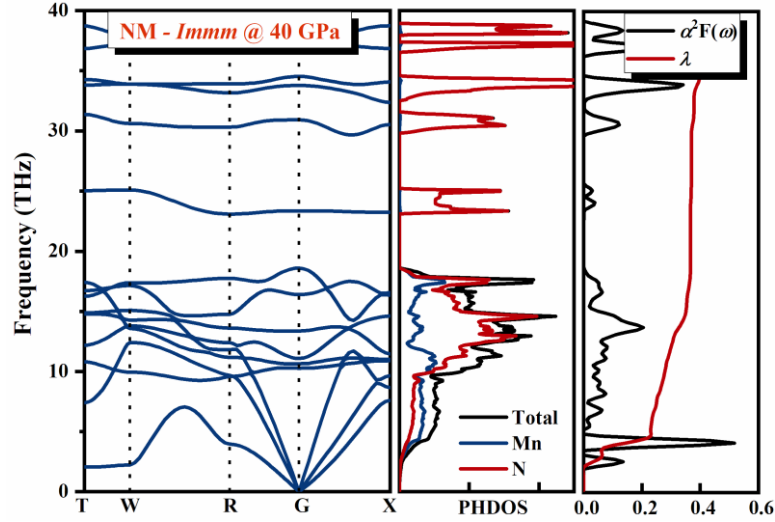


**Figure 4.** Phonon spectrum (left), PHDOS (middle), and Eliashberg spectral function  $\alpha^2F(\omega)$  together with the electron-phonon integral  $\lambda$  (right) of NM-*Immm* at 40 GPa.

### 3.3. The Phase Transformation Sequence and Electronic Properties of MnN at Pressure

Many theoretical studies on MnN have reported that the AFM *zb*-phase should be more energetically favorable than the *rs*-phase<sup>25, 40-41</sup> similar to that observed in FeN and CoN. Miao *et al* suggested that *zb*-MnN could be possibly grown under N-rich conditions by controlled doping with S, Fe, and Co; and transition from *zb* to the stable *rs* structure was observed under 4% compression.<sup>41</sup> However, there are no experimental reports on the *zb* phase in MnN until now. And the magnetic state of MnN is still discussed. Thus, we systematically studied the MnN compounds from 0 to 100 GPa according to three structural stability criteria. The *zb*, *rs*, and *NiAs* structures with their magnetic phases were fully relaxed. For the experimental AFM-*rs* phase, our study shows that lattice constant  $a = 4.17$  and  $c/a = 0.988$ , which is within the experimental values reported in literature.<sup>23</sup> This phenomenon of lattice collapse along the *c* axis is not observed in the FM or NM phases. The relative enthalpy are shown in **Figure 5a**. In terms of energy, the AFM-*zb* phase is the ground state. However, for phonon calculation (**Figure S4**), the AFM- and FM-*zb* phases are dynamically unstable, while there are no imaginary frequencies within the NM-*zb* phase. For the *rs* phase, both the FM- and AFM phases are stable at ambient pressure. Phonon spectrum reveals that the NM-*zb* phase is more stable under negative pressure (volume expansion) than under pressure. In the meantime, the phonon spectrum of the AFM-*zb* phase was calculated under negative pressure, it is still unstable. To understand this phenomenon, the electronic properties were studied (**Figure 5b, c and f**). Remarkably, the results predict the existence of a small bandgap (0.1 eV) around the Fermi level of the NM-*zb* phase, which exhibits poor metallic properties. It is attributed to the splitting of the  $e_g$ . The

$d_{x^2-y^2}$  orbital is repelled above the Fermi level, while the  $d_z^2$  orbital is pushed below the Fermi level. However, the AFM-*zb*-phase exhibits electroconductibility due to magnetic interactions, resulting in the Mn- $e_g$  orbital contribute to the Fermi level. The N–N distance are 3.013 and 3.051 Å in NM and AFM *zb*-phase, respectively. They are much larger than single bond N–N. Thus, we only performed the projected crystal orbital Hamilton population analysis (COHP) of MnN (**Figure 5d and e**) to determine the structural stability. The integrated COHP (ICOHP) analysis reconfirmed that the NM-*zb* phase (-ICOHP = 2.284) should be more stable than AFM-*zb* (-ICOHP = 2.041) owing to the higher bond strength. Under an increased pressure of ~5 GPa, the NM-*zb* phase transforms into the AFM hexagonal *NiAs* metal. This is similar to that observed with FeN:<sup>3, 42</sup> the NM-*zb* phase of FeN transforms to the FM-*NiAs* phase at ~24 GPa. When the pressure is higher than 40 GPa, AFM-*NiAs* has an imaginary phonon frequency. Thus, the FM-*rs*-phase appears, exhibiting metallicity (**Figure S6**). Interestingly, the phonon topology can be observed in the phonon spectrum of AFM-*NiAs* (**Figure S3 h and i**).

To summarize, the phase transition for MnN compounds proceeds in the following sequence: semi-conducting NM-*zb* (5 GPa) → metallic AFM-*NiAs* (40 GPa) → metallic FM-*rs*

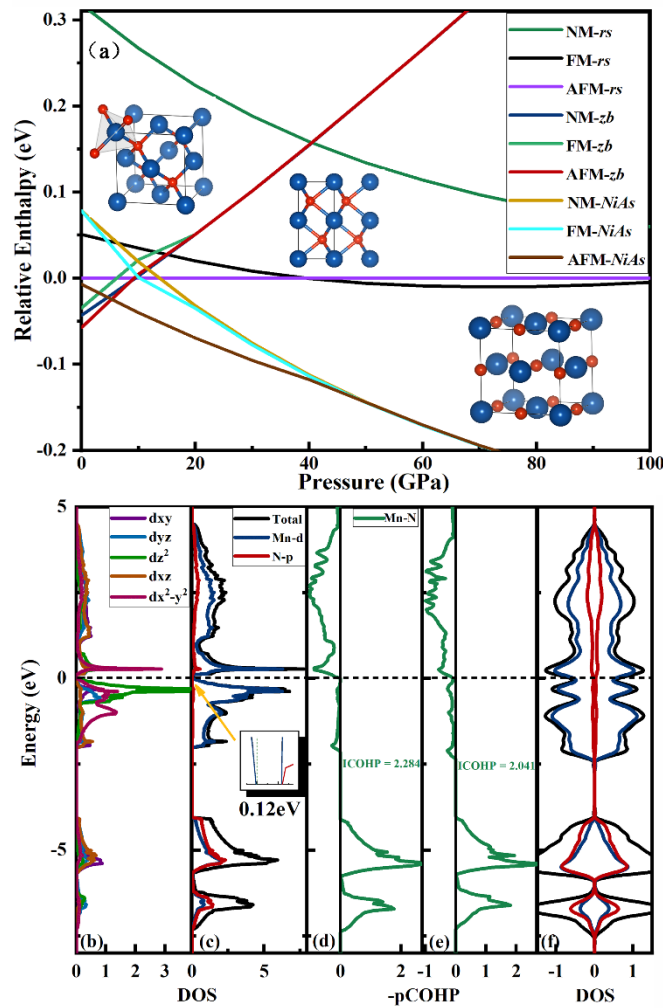


**Figure 5.** (a) The relative enthalpy of MnN and the insets are the crystal structures. (b - f) Electronic properties of *zb*-type MnN with NM and AFM phase at 0 GPa. The partial DOS and pCOHP (projected crystal orbital Hamilton population).

### 3.4. Stable Structures and Electronic Properties of Mn<sub>3</sub>N, Mn<sub>2</sub>N, and Mn<sub>3</sub>N<sub>2</sub>

Three Mn-rich phases have been predicted in NM states and exist in hexagonal layers composed of edge-sharing NMn<sub>6</sub> tri-prisms. The difference is that the hexagonal layers are separated by the Mn layers in Mn<sub>3</sub>N and form double tri-prisms layers with increasing N content in Mn<sub>3</sub>N<sub>2</sub>. In the meanwhile the crystal parameter *c* from

6.387 Å elongate to 20.672 Å. The closed N-N separations are 2.587, 2.623, and 2.626 Å for the three phases and are much longer than the N-N single bond length. The DOS evident that these phases show remarkable metallicity, the Fermi level is dominated by the Mn-3d orbital. Mn-3d and N-2p exhibit the same energy peaks (−9 and −4 eV), representing a strong interaction between the N-2p and Mn-3d states. By Bader charge transfer analysis, the per N atom of  $P\bar{6}m2$ -Mn<sub>3</sub>N obtain 1.080 e<sup>−</sup> from the Mn atoms and Mn loses more electrons with increasing nitrogen content in the three Mn-rich structures. Combine with COHP (Figure S7), the interaction between Mn and N is enhanced with increasing nitrogen content. Moreover, there are delocalized electrons between the hexagonal layers in all the three phases (Figure 6). It is a reason that they are performed metallicity.

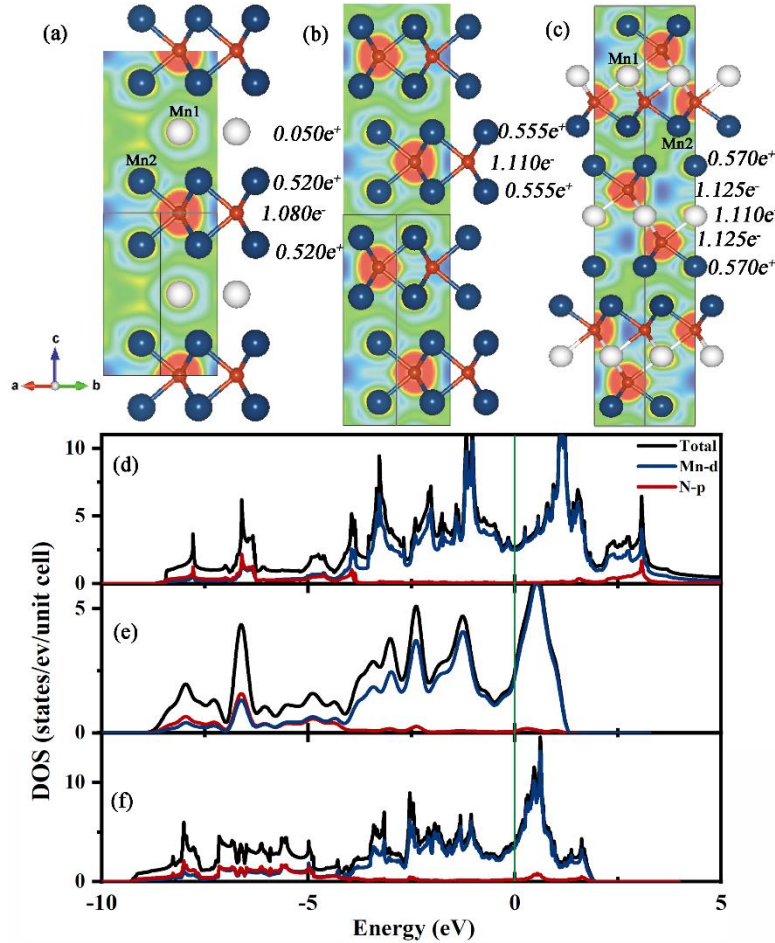


**Figure 6.** The structure diagrams, associated ELF contours (isosurface value = 0.65) and projected DOS of the (a) and (d)  $P\bar{6}m2$ -Mn<sub>3</sub>N at 0 GPa, (b) and (e)  $P6_3/mmc$ -Mn<sub>2</sub>N at 0 GPa and (c) and (f)  $R\bar{3}m$ -Mn<sub>3</sub>N<sub>2</sub> at 10 GPa.

### 3.5. Mechanical Properties of Mn–N compounds

Mechanical properties are important parameter for structural stability and the TM nitrides always perform outstanding incompressibility. Thus, the elastic moduli and hardness of all the Mn–N compounds were calculated (Figure 7 and Table S2). The hardness are been calculated by Chen’s model (Hv1)<sup>43</sup>. Due to minuscule G (39 GPa) in NM-*zb*-MnN, the hardness is negative. Moreover, in some TM light elements, the Chen's model may give a hardness value that is quite different from experiment due to the lack of consideration of the metallicity and part of the covalent bond, especially in WN<sup>44-46</sup>. On the contrary, the results of Zhong's model (Hv2) agree well with the experiment. Thus, the two models are used in this work. *Immm*-MnN<sub>4</sub> exhibits extremely high bulk modulus B (381 GPa) and shear modulus G (213 GPa), which can be comparable to *c*-BC (B = 382 GPa)<sup>47</sup>.



However, the hardness by Chen's model is 17.5 GPa. Considering the strong covalent bond and metallicity in  $\text{MnN}_4$ , the hardness is 36 GPa by Zhong's model, which is close to that of superhard materials (40 GPa). This can be attributed to the strong covalent bonds in the  $\text{N}_4$  rings. AFM- $\text{NiAs}$ - $\text{MnN}$  is also a potential hard material with hardness above 30 GPa based on Zhong's model, it may be attributed to the partially polar covalent bonds between Mn and N. The tendency of hardness is similar as the shear  $G$  with increasing in nitrogen concentration. For the three Mn-rich phases ( $\text{Mn}_3\text{N}$ ,  $\text{Mn}_2\text{N}$ , and  $\text{Mn}_3\text{N}_2$ ), the hardness obtained by the two methods was consistent. Thus, covalent interaction has a great effect on N-rich structures' hardness and hardly effect on Mn-rich structures in Mn-N compounds.

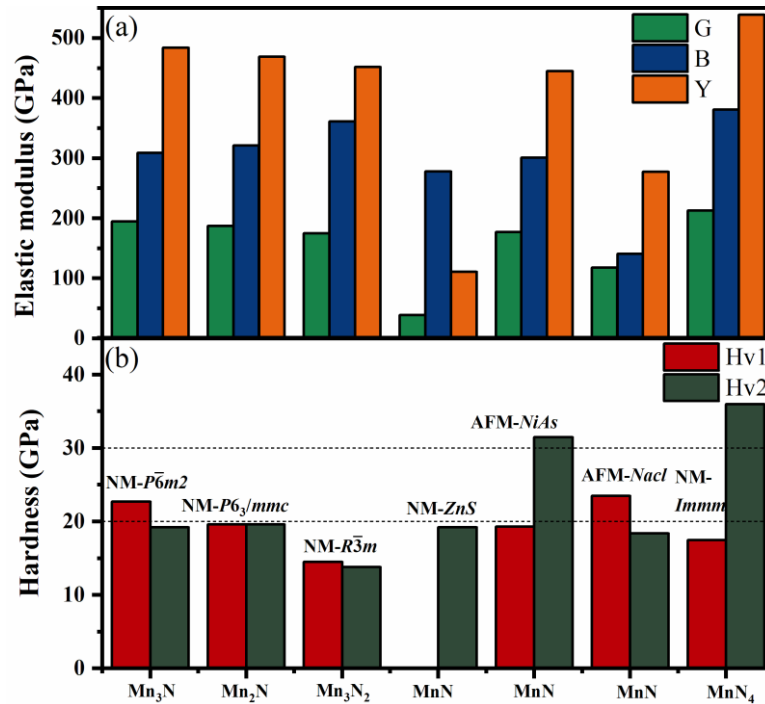


**Figure 7.** (a) Calculated bulk (B), shear (G) and Young's modulus (Y), (b) hardness for Mn-N compounds.

## Conclusions

The crystal structures of stable Mn–N compounds were investigated systematically at 0-100 GPa. A series of thermodynamically and dynamically stable Mn–N compounds were predicted for the first time. Remarkably, the planar N<sub>4</sub> rings are being reported for the first time in NM-*Immm*-MnN<sub>4</sub> with *sp*<sup>2</sup> hybridization of N; This phase with  $T_c \approx 1.6$  K and high bulk modulus  $B = 381$  GPa, which make it potentially interesting as a hard-superconductive material. The phase transition sequence for the MnN compounds is summarized renewedly. Typically, the semi-conducting NM-*zb* (5 GPa) phase transforms to the metallic AFM-*NiAs* (40 GPa), which further transforms into the more stable metallic FM-*rs* phase. AFM-*NiAs*-MnN exhibited excellent incompressibility, with hardness higher than 30 GPa, according to Zhong's model. The mechanical properties show that covalent interaction have a great effect on N-rich structures' hardness and hardly effect on Mn-rich structures in Mn–N compounds. The present findings open a new avenue for research on new superconductors in TM compounds.

## **Acknowledgements**

This work was supported by the National Key R&D Program of China (No. 2018YFA0703404, 2016YFB0201204, 2017YFA0403704), National Natural Science Foundation of China (Nos. 11774121, 91745203). Program for Changjiang Scholars and Innovative Research Team in University (No. IRT\_15R23), Parts of calculations were performed in the High Performance Computing Center (HPCC) of Jilin University.

## References

1. Salke, N. P.; Xia, K.; Fu, S.; Zhang, Y.; Greenberg, E.; Prakapenka, V. B.; Liu, J.; Sun, J.; Lin, J. F. Tungsten Hexanitride with Single-Bonded Armchairlike Hexazine Structure at High Pressure. *Phys. Rev. Lett.* **2021**, *126* (6), 065702.
2. Liu, Z.; Li, D.; Tian, F.; Duan, D.; Li, H.; Cui, T. Moderate Pressure Stabilized Pentazolate Cyclo-N5(-) Anion in Zn(N5)2 Salt. *Inorg. Chem.* **2020**, *59* (12), 8002-8012.
3. Wu, L.; Tian, R.; Wan, B.; Liu, H.; Gong, N.; Chen, P.; Shen, T.; Yao, Y.; Gou, H.; Gao, F. Prediction of Stable Iron Nitrides at Ambient and High Pressures with Progressive Formation of New Polynitrogen Species. *Chem. Mater.* **2018**, *30* (23), 8476-8485.
4. Zhang, J.; Oganov, A. R.; Li, X.; Niu, H. Pressure-stabilized hafnium nitrides and their properties. *Physical Review B* **2017**, *95* (2).
5. Zhao, Z.; Bao, K.; Tian, F.; Duan, D.; Liu, B.; Cui, T. Phase diagram, mechanical properties, and electronic structure of Nb-N compounds under pressure. *Phys. Chem. Chem. Phys.* **2015**, *17* (35), 22837-45.
6. Bhadram, V. S.; Kim, D. Y.; Strobel, T. A. High-Pressure Synthesis and Characterization of Incompressible Titanium Pernitride. *Chem. Mater.* **2016**, *28* (6), 1616-1620.
7. Baturina, T. I.; Mironov, A. Y.; Vinokur, V. M.; Baklanov, M. R.; Strunk, C. Localized superconductivity in the quantum-critical region of the disorder-driven superconductor-insulator transition in TiN thin films. *Phys. Rev. Lett.* **2007**, *99* (25), 257003.
8. Hard superconducting nitrides. *Proc. Natl. Acad. Sci. U. S. A.* **2005**.
9. Zou, Y.; Wang, X.; Chen, T.; Li, X.; Qi, X.; Welch, D.; Zhu, P.; Liu, B.; Cui, T.; Li, B. Hexagonal-structured epsilon-NbN: ultra-incompressibility, high shear rigidity, and a possible hard superconducting material. *Scientific Reports* **2015**, *5*, 10811.
10. Wang, S.; Antonio, D.; Yu, X.; Zhang, J.; Cornelius, A. L.; He, D.; Zhao, Y. The Hardest Superconducting Metal Nitride. *Scientific Reports* **2015**, *5*, 13733.
11. Zhao, Z.; Bao, K.; Tian, F.; Duan, D.; Liu, B.; Cui, T. Potentially superhard hcpCrN2 compound studied at high pressure. *Physical Review B* **2016**, *93* (21).
12. Suzuki, K.; Kaneko, T.; Yoshida, H.; Obi, Y.; Fujimori, H.; Morita, H. Crystal structure and magnetic properties of the compound MnN. *J. Alloys Compd.* **2000**, *306* (1-2), 66-71.
13. Aoki, M.; Yamane, H.; Shimada, M.; Kajiwara, T. Single crystal growth of Mn<sub>2</sub>N using an In-Na flux. *Mater. Res. Bull.* **2004**, *39* (6), 827-832.
14. Jacobs, H.; Stüve, C. Hochdrucksynthese der η-phase im system Mn-N: Mn<sub>3</sub>N<sub>2</sub>. *Journal of the Less-Common Metals* **1984**, *96* (none), 0-329.
15. Takei, W. J.; Shirane, G.; Frazer, B. C. Magnetic Structure of Mn<sub>4</sub>N. *Physical Review* **1960**, *119* (1), 122-126.
16. Li, D.; Hu, P.; Meng, M.; Li, H.; Wu, S.; Li, S. The relation of magnetic properties and anomalous Hall behaviors in Mn<sub>4</sub>N (200) epitaxial films. *Mater. Res. Bull.* **2018**, *101*, 162-166.
17. Li, H.; Wang, G.; Hu, P.; Li, D.; Dang, S.; Ma, X.; Dai, T.; Kang, S.; Yu, F.; Zhou, X.; Wu, S.; Li, S. Suppression of anomalous Hall effect by heavy-fermion in epitaxial antiperovskite Mn<sub>4-x</sub>GdxN films. *J. Appl. Phys.* **2018**, *124* (9), 093903.
18. Meinert, M. Exchange interactions and Curie temperatures of the tetrametal nitrides Cr(4)N, Mn(4)N, Fe(4)N, Co(4)N, and Ni(4)N. *J. Phys.: Condens. Matter* **2016**, *28* (5), 056006.
19. Mekata, M.; Haruna, J.; Takaki, H. Neutron Diffraction Study of Antiferromagnetic Mn<sub>2</sub>N. *J. Phys. Soc. Jpn.* **1968**, *25* (1), 234-238.
20. Hasegawa, M.; Yagi, T. Systematic study of formation and crystal structure of 3d-transition metal nitrides synthesized in a supercritical nitrogen fluid under 10 GPa and 1800K using diamond anvil cell and YAG laser heating. *J. Alloys Compd.* **2005**, *403* (1-2), 131-142.
21. Tabuchi, M.; Takahashi, M.; Kanamaru, F. Relation between the magnetic transition temperature and magnetic moment for manganese nitrides MnN<sub>γ</sub> (0 < γ < 1). *J. Alloys Compd.* **1994**, *210* (1-2), 143-148.
22. Sun, Q.; Fu, Z.-W. Mn<sub>3</sub>N<sub>2</sub> as a novel negative electrode material for rechargeable lithium batteries. *Appl. Surf. Sci.* **2012**, *258* (7), 3197-3201.

23. Suzuki, K.; Yamaguchi, Y.; Kaneko, T.; Yoshida, H.; Obi, Y.; Fujimori, H.; Morita, H. Neutron Diffraction Studies of the Compounds MnN and FeN. *J. Phys. Soc. Jpn.* **2001**.
24. Janotti, A.; Wei, S.-H.; Bellaiche, L. Electronic and magnetic properties of MnN versus MnAs. *Appl. Phys. Lett.* **2003**, *82* (5), 766-768.
25. Hong, H.-M.; Kang, Y.-J.; Kang, J.; Lee, E. C.; Kim, Y. H.; Chang, K. J. Effect of chemical bonding on the magnetic stability and magnetic moment in Mn-based binary compounds. *Physical Review B* **2005**, *72* (14).
26. Lyakhov, A. O.; Oganov, A. R.; Stokes, H. T.; Zhu, Q. New developments in evolutionary structure prediction algorithm USPEX. *Comput. Phys. Commun.* **2013**, *184* (4), 1172-1182.
27. Oganov, A. R.; Lyakhov, A. O.; Valle, M. How Evolutionary Crystal Structure Prediction Works—and Why. *Acc. Chem. Res.* **2010**, *44* (3), 227-237.
28. Kresse, G.; Furthmüller, J. Efficient iterative schemes for ab initio total-energy calculations using a plane-wave basis set. *Physical Review B* **1996**, *54* (16), 11169.
29. Kresse, G.; Joubert, D. From ultrasoft pseudopotentials to the projector augmented-wave method. *Physical Review B* **1999**, *59* (3), 1758.
30. Perdew, J. P.; Burke, K.; Ernzerhof, M. Generalized gradient approximation made simple. *Phys. Rev. Lett.* **1996**, *77* (18), 3865.
31. Monkhorst, H. J.; Pack, J. D. Special points for Brillouin-zone integrations. *Physical review B* **1976**, *13* (12), 5188.
32. Togo, A.; Oba, F.; Tanaka, I. First-principles calculations of the ferroelastic transition between rutile-type and CaCl<sub>2</sub>-type SiO<sub>2</sub> at high pressures. *Physical Review B* **2008**, *78* (13).
33. Giannozzi, P.; Baroni, S.; Bonini, N.; Calandra, M.; Car, R.; Cavazzoni, C.; Ceresoli, D.; Chiarotti, G. L.; Cococcioni, M.; Dabo, I. QUANTUM ESPRESSO: a modular and open-source software project for quantum simulations of materials. *Journal of Physics: Condensed Matter* **2009**.
34. Hill. The Elastic Behaviour of a Crystalline Aggregate. *Proceedings of the Physical Society* **1952**, *65* (5), 349-354.
35. Pickard, C. J.; Needs, R. J. High-pressure phases of nitrogen. *Phys. Rev. Lett.* **2009**, *102* (12), 125702.
36. Mekata, M. Magnetic Study on Mn<sub>4</sub>N and its Related Compounds. *J. Phys. Soc. Jpn.* **1962**, *17* (5), 796-803.
37. Huang, B.; Frapper, G. Barium–Nitrogen Phases Under Pressure: Emergence of Structural Diversity and Nitrogen-Rich Compounds. *Chem. Mater.* **2018**, *30* (21), 7623-7636.
38. Vega, D.; Almeida, D. AIM-UC: An application for QTAIM analysis. *Journal of Computational Methods in Sciences and Engineering* **2014**, *14* (1-3), 131-136.
39. Rzepa, H. The weirdest bond of all? Laplacian isosurfaces for [1.1.1]Propellane. *Henry Rzepa* **2010**.
40. Miao, M. S.; Lambrecht, W. R. L. Effects of vacancies and impurities on the relative stability of rocksalt and zincblende structures for MnN. *Physical Review B* **2007**, *76* (19).
41. Miao, M. S.; Lambrecht, W. R. L. Structure and magnetic properties of MnN, CrN, and VN under volume expansion. *Physical Review B* **2005**, *71* (21).
42. Clark, W. P.; Steinberg, S.; Dronskowski, R.; McCammon, C.; Kuppenko, I.; Bykov, M.; Dubrovinsky, L.; Akselrud, L. G.; Schwarz, U.; Niewa, R. High-Pressure NiAs-Type Modification of FeN. *Angew. Chem. Int. Ed. Engl.* **2017**, *56* (25), 7302-7306.
43. Chen, X.-Q.; Niu, H.; Li, D.; Li, Y. Modeling hardness of polycrystalline materials and bulk metallic glasses. *Intermetallics* **2011**, *19* (9), 1275-1281.
44. Zhong, M.-M.; Kuang, X.-Y.; Wang, Z.-H.; Shao, P.; Ding, L.-P.; Huang, X.-F. Phase Stability, Physical Properties, and Hardness of Transition-Metal Diborides MB<sub>2</sub> (M = Tc, W, Re, and Os): First-Principles Investigations. *The Journal of Physical Chemistry C* **2013**, *117* (20), 10643-10652.
45. Feng, X.; Bao, K.; Tao, Q.; Li, L.; Shao, Z.; Yu, H.; Xu, C.; Ma, S.; Lian, M.; Zhao, X.; Ge, Y.; Li, D.; Duan, D.; Zhu, P.; Cui, T. Role of TM-TM Connection Induced by Opposite d-Electron States on the Hardness of Transition-Metal (TM = Cr, W) Mononitrides. *Inorg. Chem.* **2019**, *58* (22), 15573-15579.
46. Xu, C.; Bao, K.; Ma, S.; Li, D.; Duan, D.; Yu, H.; Jin, X.; Tian, F.; Liu, B.; Cui, T. Revealing unusual rigid diamond net analogues in superhard titanium carbides. *RSC Advances* **2018**, *8* (26), 14479-14487.
47. Yakovenko, E.; Aleksandrov, I.; Goncharov, A.; Stishov, S. Cubic boron nitride at high pressures: equation



of state and Raman light scattering. *Zh. Eksp. Teor. Fiz.* **1989**, 95 (6), 2097-2102.